Author Manuscript
Accepted for publication in a peer-reviewed journal

NIST National Institute of Standards and Technology • U.S. Department of Commerce

Published in final edited form as:
ACS Nano. 2018 July 24; 12(7): 6612–6619. doi:10.1021/acsnano.8b01425.

Determination of Polypeptide Conformation with Nanoscale Resolution in Water

Georg Ramer[a,b,+], **Francesco Simone Ruggeri**[c,+], **Aviad Levin**[c], **Tuomas P.J. Knowles**[c,d], **Andrea Centrone**[*,a]

[a]Center for Nanoscale Science and Technology, National Institute of Standards and Technology, Gaithersburg, Maryland 20899, United States

[b]Institute for Research in Electronics and Applied Physics, University of Maryland, College Park, MD 20742, United States

[c]Department of Chemistry, University of Cambridge, Cambridge, United Kingdom, CB30FT

[d]Cavendish laboratory, Department of Physics, J J Thomson Avenue, CB3 1HE, Cambridge United Kingdom

Abstract

The folding and acquisition of native structure of proteins is central to all biological processes of life. By contrast, protein misfolding can lead to toxic amyloid aggregates formation, linked to the onset of neurodegenerative disorders. To shed light on the molecular basis of protein function and malfunction, it is crucial to access structural information of single protein assemblies and aggregates under native conditions. Yet, current conformation-sensitive spectroscopic methods lack the spatial resolution and sensitivity necessary for characterizing heterogeneous protein aggregates in solution. To overcome this limitation, here we use photothermal induced resonance (PTIR) to demonstrate that it is possible to acquire nanoscale infrared spectra in water with high signal to noise ratio (SNR). Using this approach, we probe supramolecular aggregates of diphenylalanine, the core recognition module of the Alzheimer's disease β-amyloid peptide, and its derivative Boc-diphenylalanine. We achieve nanoscale resolved IR spectra and maps in air and water with comparable SNR and lateral resolution, thus enabling accurate identification of the chemical and structural state of morphologically similar networks at the single aggregate (*i.e.* fibril) level.

Graphical Abstract

[*]**Corresponding author** Dr. A. Centrone, Center for Nanoscale Science and Technology, National Institute of Standards and Technology, Gaithersburg, Maryland 20899, United States, andrea.centrone@nist.gov.
[+]These authors contributed equally.

Author Contributions
The manuscript was written through contributions of all authors. All authors have given approval to the final version of the manuscript.

ASSOCIATED CONTENT
Supporting information
The Supporting Information is available free of charge on the ACS Publications website at
Additional information includes: PTIR measurement on PMMA coated plasmonic resonators with p-polarization, PTIR spectra of FF fibrils in air H_2O and D_2O, PTIR spectra of Boc-FF fibrils in D_2O.

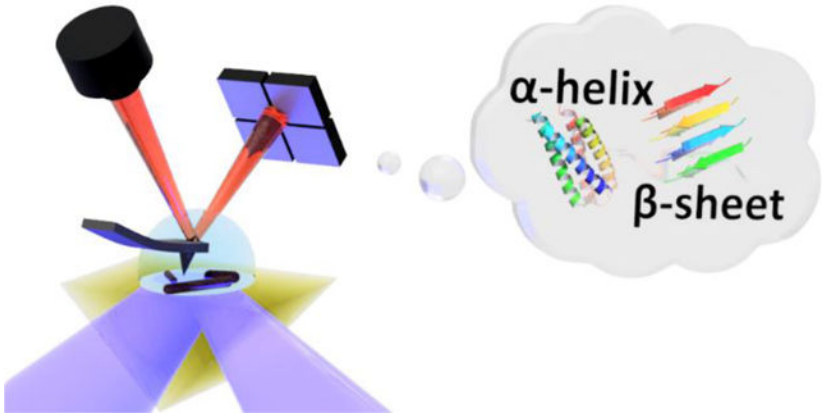

Keywords

infrared nanospectroscopy; protein aggregation; PTIR; protein structure; AFM-IR

Proteins are central to essentially all molecular processes in living organisms, and typically carry out their activities by folding into a well-defined three-dimensional structure and by binding to other molecular species to form functional complexes. Several factors, however, including high temperature, high pressure, low pH, organic solvents and natural or post-translational mutations, can steer proteins to misfolding and promote their aberrant aggregation into amyloid fibrillar structures.[1–6] Through this misfolding process, specific peptides or proteins can lose their native functional conformational state and generate toxic aggregates, which are found at the core of a broad range of human diseases, including neurodegenerative disorders such as Alzheimer's disease.[3] The development of short peptide models that adopt amyloid-like structure through hydrophobic[7] and π-π interactions[8] commonly found in amyloid structures, allow them to form supramolecular systems, which possess structural similarities to those found in amyloids. Among the wide range of self-assembling peptides, di-homopeptides, which can adopt amyloid-like fibrillar supramolecular structures, have been studied in great detail.[9, 10] Diphenylalanine, FF, the core recognition module of the Alzheimer's disease β-amyloid polypeptide, was shown to self-assemble into supramolecular systems and form nanotubes, nanospheres, nanofibrils, and hydrogels.[8, 10, 11] The formation of complex supramolecular polymers by such simple building blocks has been key for establishing FF as an archetypical model for the study of the self-assembly processes. This di-homopeptide and its analogues have allowed intense study into the mechanism underlying amyloid-related disorders propagation and their physical properties through studying their nucleation and polymerization pathway.[12] Several bulk techniques, such as Thioflavin T and Circular Dichroism have been developed to determine the structural properties of protein aggregates, yet these methods yield only average information, which is insufficient for characterizing the heterogeneous ensemble of species present in protein solutions.[4, 13–15]

Sensitive approaches for determining protein secondary and quaternary conformation and their aggregation are thus crucial to unravel their role in biological function and malfunction. An attractive approach to determine proteins' compositional and structural information

is infrared (IR) spectroscopy ensemble technique.[16] Recent advances in scanning probe techniques[17–22] have provided the ability to acquire IR spectra with nanoscale spatial resolution, which allows for the separation and determination of specific structural species in complex populations.[23,24] In particular, the photothermal induced resonance (PTIR) technique, also known as infrared nanospectroscopy (AFM-IR), has recently attracted much attention, due to the proportionality between the sample absorption coefficient and the PTIR signal,[25–28] along with the close agreement between nanoscale PTIR spectra and conventional far-field IR transmission spectra with a spatial resolution of ≈ 20 nm to ≈ 50 nm.[21, 29] These experiments have enabled nanoscale protein conformational analysis, allowing better understanding of the pathological amyloid fibrillar aggregation processes based on the determination of protein backbone conformation by the deconvolution of the conformation-sensitive Amide I band.[20, 23, 28, 30, 31] Similarly, such analysis has enabled the characterization of protein-based bio-scaffolds, carrier agents, estrogen receptors[23, 24, 30, 32–34] and of cataract diseased tissues.[35] Beyond biology, PTIR finds wide application in polymer science,[36–38] photovoltaics,[39–40] plasmonics,[26, 41–43] and pharmaceutics.[44] Moreover, the PTIR mechanical detection scheme does not restrict this method to the IR and operation in the near-IR and visible ranges have been recently demonstrated.[29, 39, 40]

While PTIR has opened a nanoscale observation window on protein conformation in heterogeneous biological systems, there is a strong need to develop measurement approaches compatible with liquid environments, which can allow gathering information that is more physiologically relevant. Yet, PTIR measurement in water are challenging[45] due to the strong IR absorption background of water (from ≈ 500 cm^{-1} to ≈ 1750 cm^{-1}, and from ≈ 2800 cm^{-1} to ≈ 3800 cm^{-1}) and because fluid drag dampens the atomic force microscopy (AFM) cantilever oscillations that yield the PTIR signal.

The first PTIR measurements in water[45] were obtained a decade ago for the *Candida Albicans* fungi with 1 μm to 2 μm thickness, by leveraging total internal reflection (TIR) illumination to minimize water direct absorption. Only recently, a second set of PTIR experiments in liquid (D_2O) was reported for polymethyl-metacrylate (PMMA) samples with nanoscale thickness (20 nm to 50 nm).[46] Measuring such thin samples in liquid required a boost of the PTIR signal-to-noise ratio (SNR), which was achieved by resonantly exciting the AFM cantilever[21] and by nano-focusing the light in the sample volume confined between a Ge prism ($n_{Ge} \approx 4.0$), and a gold coated probe.[46] Despite these sophisticated attempts, up to now, PTIR, and other nanoscale IR techniques, are considered not well suited for measurements in solution due to the low SNR achieved in practice (≈ 3.3 and ≈ 5 for the thick fungi[45] and thin PMMA[46] samples, respectively), which is insufficient for reliable band deconvolution and secondary structure identification. Because thus far PTIR data in liquid have been obtained for samples where no nanoscale absorption heterogeneities were expected, the resulting PTIR maps were either correlated or anti-correlated with the sample topography.[45, 46]

Here, we show that PTIR spectra in aqueous solutions can be obtained with high SNR (up to > 70). Furthermore, we demonstrate that PTIR maps and spectra on gold plasmonic resonators coated with a 200 nm thick PMMA layer are obtained in air and water with comparable SNR, lateral resolution and with a water absorption background that is

comparatively weak with respect to the PMMA absorption. These samples were chosen as they are characterized by heterogeneous IR absorption at the nanoscale that is not correlated with their (flat) topography.[26, 41] We further leveraged PTIR spectra in water and D_2O to detect peptide conformation on fibrillar supramolecular aggregates composed either by diphenylalanine (FF) or its tert-butoxycarbonyl (Boc)-modified derivative (Boc-FF) as model systems for amyloidogenic proteins. Along with being clinically relevant model compounds in the context of amyloid aggregation disorders, FF and Boc-FF have been chosen for this study as they yield fibrillar aggregates with similar morphology, whose different secondary structure cannot be inferred by morphology analysis alone. Thus, our results demonstrate the general capability to differentiate objects with similar morphology by their chemical and structural properties in liquid environment. We obtain IR spectra of individual nanoscale fibrillar aggregates in the Amide I, II and III bands region (hereafter named protein fingerprint region) allowing chemical and structural identification of the FF fibrils in air, water and D_2O. As these IR fingerprints, particularly the Amide band I, are related to the protein-backbone vibrations, they provide comprehensive insights into proteins secondary and quaternary structural properties. We successively measure structural differences between FF and Boc-FF fibrils, without the need for subtracting the water absorption background, thus demonstrating the ability to assess quantitatively subtle secondary and quaternary structural differences in proteins with PTIR in liquid.

Results/Discussion

PTIR, also known as AFM-IR,[17, 18] leverages narrow-band wavelength-tunable pulsed lasers for sample excitation along with an AFM probe as a near-field mechanical detector (Fig 1a) to measure IR spectra and maps with sub 20 nm spatial resolution.[21, 29] Although PTIR setups that illuminate the sample from the air phase are common,[18] measurements in the liquid phase require sample illumination in total internal reflection (TIR) using an optical prism, ZnSe in this work, to curb the water absorption background. In PTIR, the AFM probe transduces the light-induced thermal expansion of the sample into cantilever oscillations that are detected by the AFM detector. Si_3N_4 triangular AFM probes, without a metallic coating, were used in this work, demonstrating that high SNR is achievable in water even without resorting to the tip-induced field-enhancement typically provided by gold-coated probes. PTIR experiments in this work were obtained using s-polarized light, with the exception of the data reported in Figure S1.

PTIR absorption maps are obtained by scanning the AFM cantilever on the sample surface, while maintaining the laser wavelength fixed. Whereas, PTIR spectra are obtained by sweeping the laser wavelength maintaining the position of the AFM cantilever fixed. Through tuning of the PTIR laser repetition rate to match one of the cantilever oscillation frequencies, it is possible to increase the PTIR signal amplitude by the cantilever mode Q-factor,[21] which is very effective in air (high Q-factors),[21] as shown in Fig 1b. In liquid, this mode of operation is key for obtaining PTIR data with sufficient SNR, although the fluid drag strongly dampens the AFM cantilever oscillations, thus reducing the Q-factors significantly (Fig 1b).

To demonstrate the ability of capturing high quality PTIR data in water we first obtained and compared data on an array made of gold asymmetric split ring resonators (ASSRs)[26, 41, 42] coated with 200 nm PMMA film either in air or in water (Fig. 2). We chose this sample for several reasons. First, previous extensive PTIR characterization in air have shown that similar samples exhibit spatially heterogeneous absorption at the nanoscale.[26, 41, 42, 47] Second, since the sample displays only small variations in thickness, the correlation between a spatially heterogeneous absorption and sample thickness (*i.e.* topography) can be excluded. Third, as the sample top layer is chemically homogenous, possible artefacts due heterogeneity of the tip-sample mechanical contact[48, 49] (*i.e.* possible sensitivity of the PTIR signal to the sample mechanical properties) can be excluded. The ASSRs studied here have plasmon resonances of ≈ 9 μm and were fabricated by electron-beam lithography and lift-off on a ZnSe prism.[41] The ASSRs have a diameter of 1750 nm ± 50 nm, thickness of 180 nm ± 10 nm and a pitch of 3012 nm ± 22 nm, as determined by AFM. After the deposition of the top PMMA layer, the sample shows an AFM maximum topographic variation of 70 nm ± 10 nm. The uncertainties throughout the manuscript represent a single standard deviation in the measurements on nominally identical resonators. The surface plasmon resonance (SPR) is a characteristic optical resonant response observed in noble metal nanostructures, which can be engineered by controlling the structure, composition size and shape.[50, 51] The nanoscale confinement of light, which promote locally enhanced light-matter interactions is one of the most studied benefits provided by SPRs.[41, 50–52] For example, in the mid-IR, SPRs can be exploited for chemical identification by boosting the sensitivity of IR spectroscopy, an effect known as surface enhanced infrared absorption (SEIRA).[26, 41, 50, 51, 53] The AFM topography maps in air (Fig 2a) and water (Fig 2b) are quite similar and show the topographic outlines of the buried resonators and that the sample surface is rather flat. The PTIR maps (s-polarization 1188 cm^{-1}, corresponding to vibrations of the ester group of PMMA) in air (Fig 2c) or water (Fig 2d) display the SEIRA enhancement (hot spots) arising from the field confinement near the resonators gaps.[26, 41] These images, obtained using a phase locked loop (PLL, see methods), demonstrate that PTIR imaging in water can be achieved without significant difference of resolution or SNR (≈ 17 and ≈ 35 in air and water, respectively). Similar conclusions can be derived from the PTIR data obtained with p-polarization (see Fig S1). Although the lower Q-factors in water limit the effectiveness of the cantilever resonant excitation for amplifying the PTIR signal, they increase the bandwidth over which the PLL can effectively track the cantilever resonance, which is key for obtaining high quality images with this method. In Fig. 2 the SNR of the PTIR image in water exceeds the one in air because the chosen AFM probe is well adapted to water operation and because of the broader bandwidth over which the PLL is effective in water. Representative PTIR spectra of PMMA obtained in the hot spot locations (Fig 2e), also display high SNR (235 ± 13 and 70 ± 7 in air and water respectively). Comparison with the PMMA spectrum in water (Fig 2e), obtained away from the resonator, reveals SEIRA enhancement factors up to ≈ 30 in the hot-spot locations.

Having tested the PTIR capabilities in liquid on PMMA, we next characterize diphenylalanine (FF) supramolecular fibrillar aggregates as a model system to assess the capability to resolve chemical signatures and conformation of the polypeptide in water. FF, the core recognition module of the Alzheimer's disease β-amyloid polypeptide and its Boc

modified analogue were shown to self-assemble into supramolecular systems and form a wide array of ordered structures,[11, 54] thus establishing FF as an archetypical model for the study of the fundamental principles governing the self-assembly process of proteins. In Figure 3, we show characteristic AFM morphology and PTIR absorption (1615 cm^{-1}) maps of FF nanotubes with nanoscale diameter in air (Fig.3a and SI Fig. 2) and in water (Fig.3b and SI Fig. 3). The comparison of the IR maps in air and in water demonstrates that PTIR imaging in the liquid phase does not lead to a significant loss in spatial resolution, in agreement with the measurement on PMMA. PTIR spectra at selected locations on the fibrillar samples cover the Amide I (1700 cm^{-1} to 1600 cm^{-1}), amide II (1580 cm^{-1} to 1500 cm^{-1}), to C-C ring vibrations and partially to Amide III (1500 cm^{-1} to 1400 cm^{-1}) regions both in air and in water (SI Fig. 2–4). As shown in Fig. 3c, the spectra in water and in air show a high degree of similarity along the whole protein fingerprint spectral range and match previous data reported in literature.[55] A more accurate comparison of the spectroscopic signatures can be obtained evaluating the second derivatives of the PTIR spectra (Fig. 3d). In the Amide band I region, both in water and in air, we can observe a sharp peak (1690 cm^{-1}) that corresponds to antiparallel β-sheet conformation. The spectra present a slightly different shape between 1640 cm^{-1} and 1600 cm^{-1}, a variation that can be associated to changes in the hydration state of the NH_3^+ groups (absorption at ≈ 1600 cm^{-1}) and to the presence of residual water absorption (between 1640 cm^{-1} and 1600 cm^{-1}) within the nanotubes. The Amide II band shows absorption peaks at 1555 cm^{-1} and 1520 cm^{-1}. As the Amide II absorbance arises from NH vibrations, the small spectral differences in this region can be again related to the different hydration state of the sample when in air or liquid. Along with the amide bands, sharp bands associated to C-C ring vibrations at 1605 cm^{-1}, 1495 cm^{-1}, 1452 cm^{-1} and 1430 cm^{-1} are observed in the spectra. Due to the high quality PTIR data in water, the chemical signature and structural conformation of the FF fibrillar aggregates at the nanoscale can be determined with confidence. Similarly, it is possible to identify chemically and structurally the FF fibrils in liquid D_2O environment (SI Fig. 4). This is not surprising, as D_2O is commonly used to avoid spectral overlap between amide IR absorption bands and the H_2O absorption.

To assess further the PTIR capabilities in liquid, we focused on the Amide I vibrational signatures to investigate the structural differences between FF and Boc-FF nanotube aggregates (see AFM morphology in Fig 4a–b). The FF and the Boc-FF peptides chemical structures (Fig. 4a–b) only differ by the presence of the *tert*-butyloxycarbonyl group. To determine their secondary structure, and to rule out any possible influence related to the water absorption background on the conformational analysis due to partial spectral overlap, the aggregates were formed in D_2O. We could easily obtain chemical information from individual fibrillar aggregates with diameters smaller than 200 nm (SI Fig. 2, 5, 6). In Fig. 4c, we show the PTIR spectra comparison of the Amide band I region highlighting the different backbone structures of the two fibrillar aggregates. As expected based on the different chemical structure, spectra of the Boc-FF aggregates show an increased absorption at 1730 cm^{-1} due to the additional carboxylic group with respect to the FF fibrils. Boc-FF also possesses a carbamate group absorbing at 1696 cm^{-1},[55] which overlaps with the antiparallel β-sheet absorption and contributes to a shift of the amide I band towards higher wavenumbers, thus justifying the different position of this structural-sensitive feature

between Boc-FF and FF aggregates. Finally, as the presence of the *tert*-Butyloxycarbonyl group confers a larger conformational freedom with respect to FF, the Boc-FF fibrils spectrum exhibits an additional amide I contribution (1664 cm^{-1} to 1655 cm^{-1}), that is related to the α-helix and 3-helix conformations. This analysis was confirmed by the observation of the second derivatives of the spectra (Fig 4d).

Conclusions

To conclude, we demonstrate the identification of the chemical signature of individual fibrillar aggregates measured in water at the nanoscale, enabling the determination and comparison of their secondary structural conformation. Our data confirm that the FF and Boc-FF fibrils differ structurally at the individual fibril level due to the presence of α-helical conformation of the Boc-FF with respect to the pure β-sheet conformation of FF. This highly sensitive and nanoscale-resolved characterization can thus be further applied for studies of more complex aggregating systems in water. We believe that the development of advanced biophysical methodologies, capable of bridging morphological and structural properties investigations of amyloid-like aggregates at the nanoscale, represents a fruitful avenue to address the challenges of fully understanding protein self-assembly, to unravel monomer misfolding and to elucidate the molecular mechanisms of neurodegeneration. Furthermore, as an ever-growing class of functional amyloids has been recently found to occur naturally in disease-unrelated biological processes and as many artificial peptides can form amyloid-like structures *in-vitro*, we believe this work will influence protein research in a broad set of applications. Finally, recently introduced nano-sized AFM probes leveraging integrated cavity opto-mechanics that yield significantly increased PTIR sensitivity, time resolution and throughput,[22] hold further promise for an improved PTIR performance in liquid thanks to a much reduced cantilever drag.

Methods/Experimental

PTIR sample preparation and deposition. H-L-Phe-L-Phe-COOH (FF) was dissolved in H_2O and D_2O at a concentration of 1 mg/ml to form supramolecular aggregates as previously reported.[56] N-(tert-butoxycarbonyl)-L-Phe-L-Phe-COOH (Boc-FF) stock solutions at a concentration of 10 mg/ml were prepared in absolute EtOH and then diluted at a ratio of 1:10 in H_2O and D_2O to allow formation of aggregates as previously reported.[11] An aliquot of each sample was deposit on a hydrophobic ZnSe prism for further analysis.[23, 57]

PTIR data acquisition. A modified commercial PTIR setup[29] using TIR illumination and interfaced with an external-cavity quantum cascade laser (EC-QCL) array covering the spectral range from 769 cm^{-1} to 1763 cm^{-1} was used for the PTIR experiments. The repetition rate of the EC-QCL source (tunable between 0.1 kHz and 2000 kHz) was set to match one of the cantilever oscillation mode in air or liquid (see fig 1b) to resonantly exciting the AFM cantilever (resonance-enhanced PTIR).[21] For imaging a phase locked loop (PLL) was used to maintain the contact resonance excitation condition throughout the measurement. The samples were deposited from solution onto right angle ZnSe prism substrates. Triangular Si_3N_4 cantilevers with a nominal length of 120 μm ± 5 μm and a first resonance frequency (non-contact in air) of 65 kHz ± 15 kHz, were used in the PTIR

experiments. After deposition, the sample solution was replenished with a syringe filled with either H_2O or D_2O as needed. In the experiments both the sample and the AFM cantilever were completely immersed in the liquid. The PTIR instrument was operated in ambient atmosphere without precautions to prevent hydrogen-deuterium exchange of the liquid phase with ambient humidity during the measurement. PTIR data analysis. PTIR spectra on PMMA are averages of 5 single spectra taken at the same location. No further data processing was performed. The SNR in the PTIR spectra was determined as the ratio of the PTIR intensity at 1160 cm^{-1} and the standard deviation of the PTIR signal in the range between 1510 cm^{-1} and 1560 cm^{-1} where the PMMA spectrum is typically flat. The uncertainties of the SNR were calculated as the standard deviation of the SNRs of five spectra measured under the same conditions. The SEIRA enhancement was determined as the ratio of the PTIR intensity at the hotspot locations with respect to the intensity of the PTIR spectrum away from the resonators. Before calculating the ratio, five PTIR spectra were averaged and then smoothed, using a finite impulse response digital filter.

The SNR in PTIR images of the plasmonic resonators was determined as the ratio of the maximum PTIR amplitude value and the standard deviation of the PTIR amplitude away from the hotspots.

The spectra of the peptides were processed first by averaging at least 10 nominally identical spectra obtained in a given sample position. To remove the water contribution from the FF spectra, a reference spectrum was obtained with the AFM in contact with the substrate (water background spectrum). The two spectra are first normalized to their maximum intensities and then either subtracted or divided leading to similar results (SI Fig. 3). Later the spectra were smoothed by adjacent averaging (3 points) Savitzky-Golay filter (2^{nd} order, 12 points) and finally their maximum intensities were normalised to one for comparison. For band deconvolution, second derivative spectra (2^{nd} order, 9 points) were calculated from the normalized spectra. All these operations were carried out in a commercial statistics software package.

Supplementary Material

Refer to Web version on PubMed Central for supplementary material.

ACKNOWLEDGEMENTS

GR acknowledges support under the Cooperative Research Agreement between the University of Maryland and the National Institute of Standards and Technology Center for Nanoscale Science and Technology, Award 70NANB14H209, through the University of Maryland. This work is supported by the Swiss National Science Foundation (F.S.R., grant number P2ELP2_162116 & P300P2_171219).

REFERENCES

1. Chiti F; Dobson CM, Protein Misfolding, Functional Amyloid, and Human Disease. Annu. Rev. Biochem. 2006, 75, 333–366. [PubMed: 16756495]
2. Dobson CM, Protein Folding and Misfolding. Nature 2003, 426, 884–890. [PubMed: 14685248]
3. Knowles TPJ; Vendruscolo M; Dobson CM, The Amyloid State and Its Association with Protein Misfolding Diseases. Nat. Rev. Mol. Cell Biol. 2014, 15, 384–396. [PubMed: 24854788]

4. Stefani M; Dobson CM, Protein Aggregation and Aggregate Toxicity: New Insights into Protein Folding, Misfolding Diseases and Biological Evolution. J. Mol. Med. 2003, 81, 678–699. [PubMed: 12942175]
5. Soto C, Unfolding the Role of Protein Misfolding in Neurodegenerative Diseases. Nat. Rev. Neurosci. 2003, 4, 49–60. [PubMed: 12511861]
6. Dobson CM, Protein Misfolding, Evolution and Disease. Trends Biochem. Sci. 1999, 24, 329–332. [PubMed: 10470028]
7. Mart RJ; Osborne RD; Stevens MM; Ulijn RV, Peptide-Based Stimuli-Responsive Biomaterials. Soft Matter 2006, 2, 822–835 [PubMed: 32680274]
8. Orbach R; Mironi-Harpaz I; Adler-Abramovich L; Mossou E; Mitchell EP; Forsyth VT; Gazit E; Seliktar D, The Rheological and Structural Properties of Fmoc-Peptide-Based Hydrogels: The Effect of Aromatic Molecular Architecture on Self-Assembly and Physical Characteristics. Langmuir 2012, 28, 2015–2022. [PubMed: 22220968]
9. Gazit E, A Possible Role for Pi-Stacking in the Self-Assembly of Amyloid Fibrils. FASEB J. 2002, 16, 77–83. [PubMed: 11772939]
10. Reches M; Gazit E, Designed Aromatic Homo-Dipeptides: Formation of Ordered Nanostructures and Potential Nanotechnological Applications. Phys. Biol. 2006, 3, S10–S19. [PubMed: 16582461]
11. Levin A; Mason TO; Adler-Abramovich L; Buell AK; Meisl G; Galvagnion C; Bram Y; Stratford SA; Dobson CM; Knowles TP; Gazit E, Ostwald's Rule of Stages Governs Structural Transitions and Morphology of Dipeptide Supramolecular Polymers. Nat. Commun. 2014, 5, 5219. [PubMed: 25391268]
12. Mason TO; Michaels TCT; Levin A; Dobson CM; Gazit E; Knowles TPJ; Buell AK, Thermodynamics of Polypeptide Supramolecular Assembly in the Short-Chain Limit. J. Am. Chem. Soc. 2017, 139, 16134–16142. [PubMed: 28994295]
13. Ruggeri FS; Adamcik J; Jeong JS; Lashuel HA; Mezzenga R; Dietler G, Influence of the B-Sheet Content on the Mechanical Properties of Aggregates During Amyloid Fibrillization. Angew. Chem., Int. Ed. 2015, 127, 2492–2496.
14. Zandomeneghi G; Krebs MR; McCammon MG; Fandrich M, FTIR Reveals Structural Differences between Native Beta-Sheet Proteins and Amyloid Fibrils. Protein Sci. 2004, 13, 3314–21. [PubMed: 15537750]
15. Whitmore L; Wallace BA, Protein Secondary Structure Analyses from Circular Dichroism Spectroscopy: Methods and Reference Databases. Biopolymers 2008, 89, 392–400. [PubMed: 17896349]
16. Barth A, Infrared Spectroscopy of Proteins. Biochim. Biophys. Acta, Bioenerg. 2007, 1767, 1073–101.
17. Centrone A, Infrared Imaging and Spectroscopy Beyond the Diffraction Limit. Annu. Rev. Anal. Chem. 2015, 8, 101–126.
18. Dazzi A; Prater CB, AFM-IR: Technology and Applications in Nanoscale Infrared Spectroscopy and Chemical Imaging. Chem. Rev. 2017, 117, 5146–5173. [PubMed: 27958707]
19. Xiao L; Schultz ZD, Spectroscopic Imaging at the Nanoscale: Technologies and Recent Applications. Anal. Chem. 2017, 90, 440–458. [PubMed: 29028297]
20. Ruggeri FS; Habchi J; Cerreta A; Dietler G, AFM-Based Single Molecule Techniques: Unraveling the Amyloid Pathogenic Species. Curr. Pharm. Des. 2016, 22, 3950–3970. [PubMed: 27189600]
21. Lu F; Jin MZ; Belkin MA, Tip-Enhanced Infrared Nanospectroscopy Via Molecular Expansion Force Detection. Nat. Photonics 2014, 8, 307–312.
22. Chae J; An S; Ramer G; Stavila V; Holland G; Yoon Y; Talin AA; Allendorf M; Aksyuk VA; Centrone A, Nanophotonic Atomic Force Microscope Transducers Enable Chemical Composition and Thermal Conductivity Measurements at the Nanoscale. Nano Lett. 2017, 17, 5587–5594. [PubMed: 28770607]
23. Ruggeri FS; Longo G; Faggiano S; Lipiec E; Pastore A; Dietler G, Infrared Nanospectroscopy Characterization of Oligomeric and Fibrillar Aggregates During Amyloid Formation. Nat. Commun. 2015, 6, 7831. [PubMed: 26215704]

24. Galante D; Ruggeri FS; Dietler G; Pellistri F; Gatta E; Corsaro A; Florio T; Perico A; D'Arrigo C, A Critical Concentration of N-Terminal Pyroglutamylated Amyloid Beta Drives the Misfolding of Ab1–42 into More Toxic Aggregates. Int. J. Biochem. Cell Biol. 2016, 79, 261–270. [PubMed: 27592450]
25. Dazzi A; Glotin F; Carminati R, Theory of Infrared Nanospectroscopy by Photothermal Induced Resonance. J. Appl. Phys. 2010, 107, 124519.
26. Lahiri B; Holland G; Aksyuk V; Centrone A, Nanoscale Imaging of Plasmonic Hot Spots and Dark Modes with the Photothermal-Induced Resonance Technique. Nano Lett. 2013, 13, 3218–3224. [PubMed: 23777547]
27. Tang F; Bao P; Su Z, Analysis of Nanodomain Composition in High-Impact Polypropylene by Atomic Force Microscopy-Infrared. Anal. Chem. 2016, 88, 4926–4930. [PubMed: 27075757]
28. Ramer G; Aksyuk VA; Centrone A, Quantitative Chemical Analysis at the Nanoscale Using the Photothermal Induced Resonance Technique. Anal. Chem. 2017, 89, 13524–13531. [PubMed: 29165992]
29. Katzenmeyer AM; Holland G; Kjoller K; Centrone A, Absorption Spectroscopy and Imaging from the Visible through Mid-Infrared with 20 nm Resolution. Anal. Chem. 2015, 87, 3154–3159. [PubMed: 25707296]
30. Ruggeri FS; Vieweg S; Cendrowska U; Longo G; Chiki A; Lashuel HA; Dietler G, Nanoscale Studies Link Amyloid Maturity with Polyglutamine Diseases Onset. Sci. Rep. 2016, 6, 31155. [PubMed: 27499269]
31. Qamar S; Wang G; Randle SJ; Ruggeri FS; Varela JA; Lin JQ; Phillips EC; Miyashita A; Williams D; Strohl F; Meadows W; Ferry R; Dardov VJ; Tartaglia GG; Farrer LA; Kaminski Schierle GS; Kaminski CF; Holt CE; Fraser PE; Schmitt-Ulms G, et al. , Fus Phase Separation Is Modulated by a Molecular Chaperone and Methylation of Arginine Cation-Pi Interactions. Cell 2018, 173, 720–734 e15. [PubMed: 29677515]
32. Muller T; Ruggeri FS; Kulik AJ; Shimanovich U; Mason TO; Knowles TPJ; Dietler G, Nanoscale Spatially Resolved Infrared Spectra from Single Microdroplets. Lab Chip 2014, 14, 1315–1319. [PubMed: 24519414]
33. Ruggeri FS; Byrne C; Khemtemourian L; Ducouret G; Dietler G; Jacquot Y, Concentration-Dependent and Surface-Assisted Self-Assembly Properties of a Bioactive Estrogen Receptor Alpha-Derived Peptide. J. Pept. Sci. 2015, 21, 95–104. [PubMed: 25530026]
34. Volpatti LR; Shimanovich U; Ruggeri FS; Bolisetty S; Muller T; Mason TO; Michaels TCT; Mezzenga R; Dietler G; Knowles TPJ, Micro- and Nanoscale Hierarchical Structure of Core-Shell Protein Microgels. J. Mater. Chem. B 2016, 4, 7989–7999. [PubMed: 32263788]
35. Paluszkiewicz C; Piergies N; Chaniecki P; Rekas M; Miszczyk J; Kwiatek WM, Differentiation of Protein Secondary Structure in Clear and Opaque Human Lenses: AFM - IR Studies. J. Pharm. Biomed. Anal. 2017, 139, 125–132. [PubMed: 28279927]
36. Gong L; Chase DB; Noda I; Marcott CA; Liu J; Martin DC; Ni C; Rabolt JF, Polymorphic Distribution in Individual Electrospun Poly[(R)-3-Hydroxybutyrate-Co-(R)-3-Hydroxyhexanoate] (Phbhx) Nanofibers. Macromolecules 2017, 50, 5510–5517.
37. Morsch S; Liu YW; Lyon SB; Gibbon SR, Insights into Epoxy Network Nanostructural Heterogeneity Using AFM-IR. ACS Appl. Mater. Interfaces 2016, 8, 959–966. [PubMed: 26694687]
38. Tri PN; Prud'homme RE, Nanoscale Lamellar Assembly and Segregation Mechanism of Poly(3-Hydroxybutyrate)/Poly(Ethylene Glycol) Blends. Macromolecules 2018, 51, 181–188.
39. Strelcov E; Dong Q; Li T; Chae J; Shao Y; Deng Y; Gruverman A; Huang J; Centrone A, Ch3nh3pbi3 Perovskites: Ferroelasticity Revealed. Sci. Adv. 2017, 3, e1602165. [PubMed: 28439542]
40. Chae J; Dong Q; Huang J; Centrone A, Chloride Incorporation Process in Ch(3)Nh(3)Pbi(3-X)Cl(X) Perovskites Via Nanoscale Bandgap Maps. Nano Lett. 2015, 15, 8114–8121. [PubMed: 26528710]
41. Chae J; Lahiri B; Centrone A, Engineering near-Field SEIRA Enhancements in Plasmonic Resonators. ACS Photonics 2016, 3, 87–95. [PubMed: 27182532]

42. Katzenmeyer AM; Chae J; Kasica R; Holland G; Lahiri B; Centrone A, Nanoscale Imaging and Spectroscopy of Plasmonic Modes with the PTIR Technique. Adv. Opt. Mater. 2014, 2, 718–722.
43. Khanikaev AB; Arju N; Fan Z; Purtseladze D; Lu F; Lee J; Sarriugarte P; Schnell M; Hillenbrand R; Belkin MA; Shvets G, Experimental Demonstration of the Microscopic Origin of Circular Dichroism in Two-Dimensional Metamaterials. Nat. Commun. 2016, 7, 12045. [PubMed: 27329108]
44. Van Eerdenbrugh B; Lo M; Kjoller K; Marcott C; Taylor LS, Nanoscale Mid-Infrared Imaging of Phase Separation in a Drug-Polymer Blend. J. Pharm. Sci. 2012, 101, 2066–2073. [PubMed: 22388948]
45. Mayet C; Dazzi A; Prazeres R; Allot E; Glotin E; Ortega JM, Sub-100 nm IR Spectromicroscopy of Living Cells. Opt. Lett. 2008, 33, 1611–1613. [PubMed: 18628814]
46. Jin M; Lu F; Belkin MA, High-Sensitivity Infrared Vibrational Nanospectroscopy in Water. Light: Sci. Appl. 2017, 6, e17096. [PubMed: 30167276]
47. Chae J; Lahiri B; Kohoutek J; Holland G; Lezec H; Centrone A, Metal-Dielectric-Metal Resonators with Deep Subwavelength Dielectric Layers Increase the near-Field SEIRA Enhancement. Opt. Express 2015, 23, 25912–25922. [PubMed: 26480106]
48. Barlow DE; Biffinger JC; Cockrell-Zugell AL; Lo M; Kjoller K; Cook D; Lee WK; Pehrsson PE; Crookes-Goodson WJ; Hung CS; Nadeau LJ; Russell JN, The Importance of Correcting for Variable Probe-Sample Interactions in AFM-IR Spectroscopy: AFM-IR of Dried Bacteria on a Polyurethane Film. Analyst 2016, 141, 4848–4854. [PubMed: 27403761]
49. Ramer G; Reisenbauer F; Steindl B; Tomischko W; Lendl B, Implementation of Resonance Tracking for Assuring Reliability in Resonance Enhanced Photothermal Infrared Spectroscopy and Imaging. Appl. Spec. 2017, 71, 2013–2020.
50. Mayerhofer TG; Popp J, Periodic Array-Based Substrates for Surfaceenhanced Infrared Spectroscopy. Nanophotonics 2018, 7, 39–79.
51. Neubrech F; Huck C; Weber K; Pucci A; Giessen H, Surface-Enhanced Infrared Spectroscopy Using Resonant Nanoantennas. Chem. Rev. 2017, 117, 5110–5145. [PubMed: 28358482]
52. Bailo E; Deckert V, Tip-Enhanced Raman Scattering. Chem. Soc. Rev. 2008, 37, 921–930. [PubMed: 18443677]
53. Etezadi D; Warner IV JB; Ruggeri FS; Dietler G; Lashuel HA; Altug H, Nanoplasmonic Mid-Infrared Biosensor for in Vitro Protein Secondary Structure Detection. Light: Sci. Appl. 2017, 6, e17029.
54. Reches M; Gazit E, Self-Assembly of Peptide Nanotubes and Amyloid-Like Structures by Charged-Termini-Capped Diphenylalanine Peptide Analogues. Isr. J. Chem. 2005, 45, 363–371.
55. Creasey RCG; Louzao I; Arnon ZA; Marco P; Adler-Abramovich L; Roberts CJ; Gazit E; Tendler SJB, Disruption of Diphenylalanine Assembly by a Boc-Modified Variant. Soft Matter 2016, 12, 9451–9457. [PubMed: 27841428]
56. Mason TO; Chirgadze DY; Levin A; Adler-Abramovich L; Gazit E; Knowles TP; Buell AK, Expanding the Solvent Chemical Space for Self-Assembly of Dipeptide Nanostructures. ACS Nano 2014, 8, 1243–1253. [PubMed: 24422499]
57. Jeon JS; Raghavan S; Sperline RP, Quantitative Analysis of Albumin Adsorption onto Uncoated and Poly(Ether)Urethane-Coated Znse Surfaces Using the Attenuated Total Reflection FTIR Technique. Colloids Surf., A 1994, 92, 255–265.

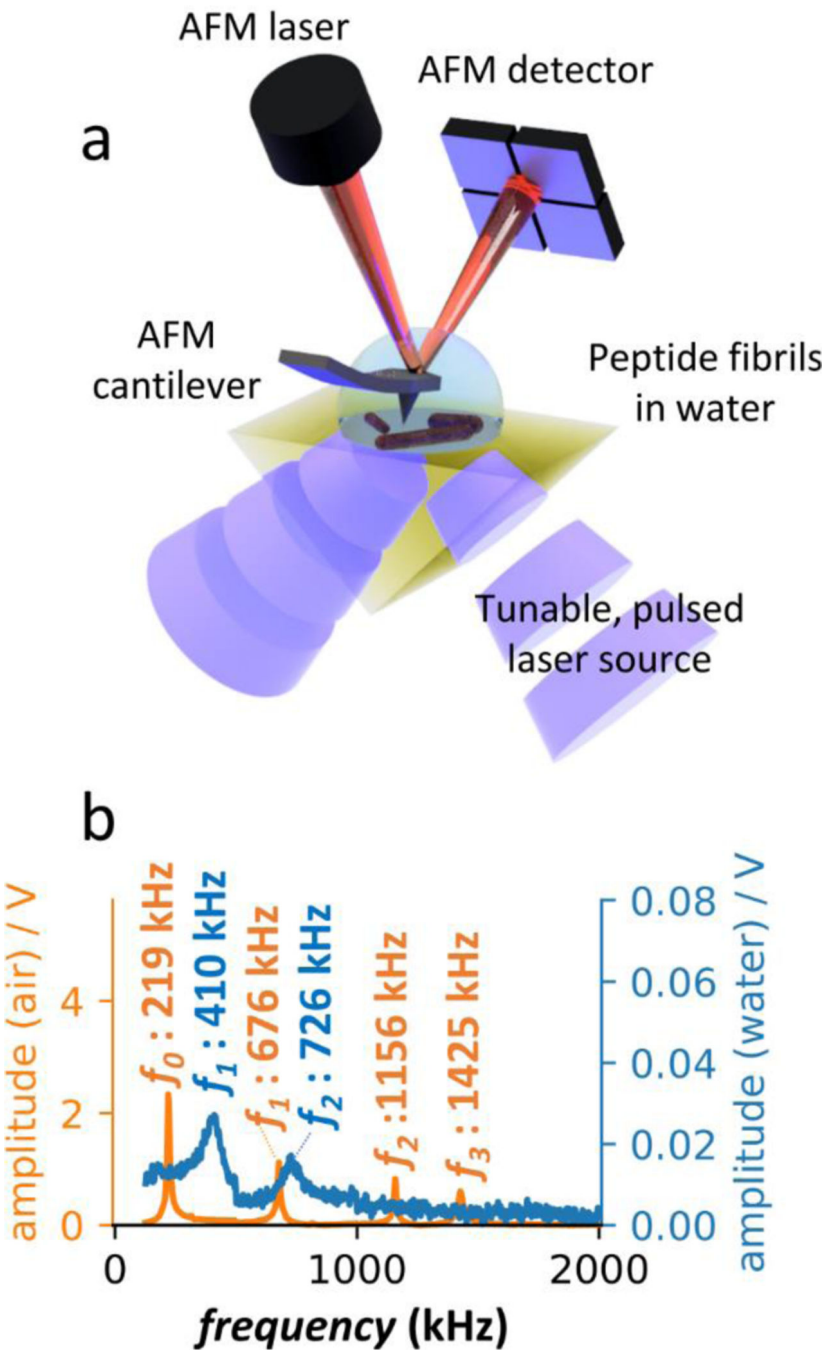

Figure 1. PTIR set up in water.

a) PTIR measurement schematic. The sample is illuminated from below in TIR configuration. The AFM cantilever transduces the photo-induced thermal expansion of the sample as measured by the AFM detector. b) AFM cantilever contact resonant frequencies in air (orange) and water (blue).

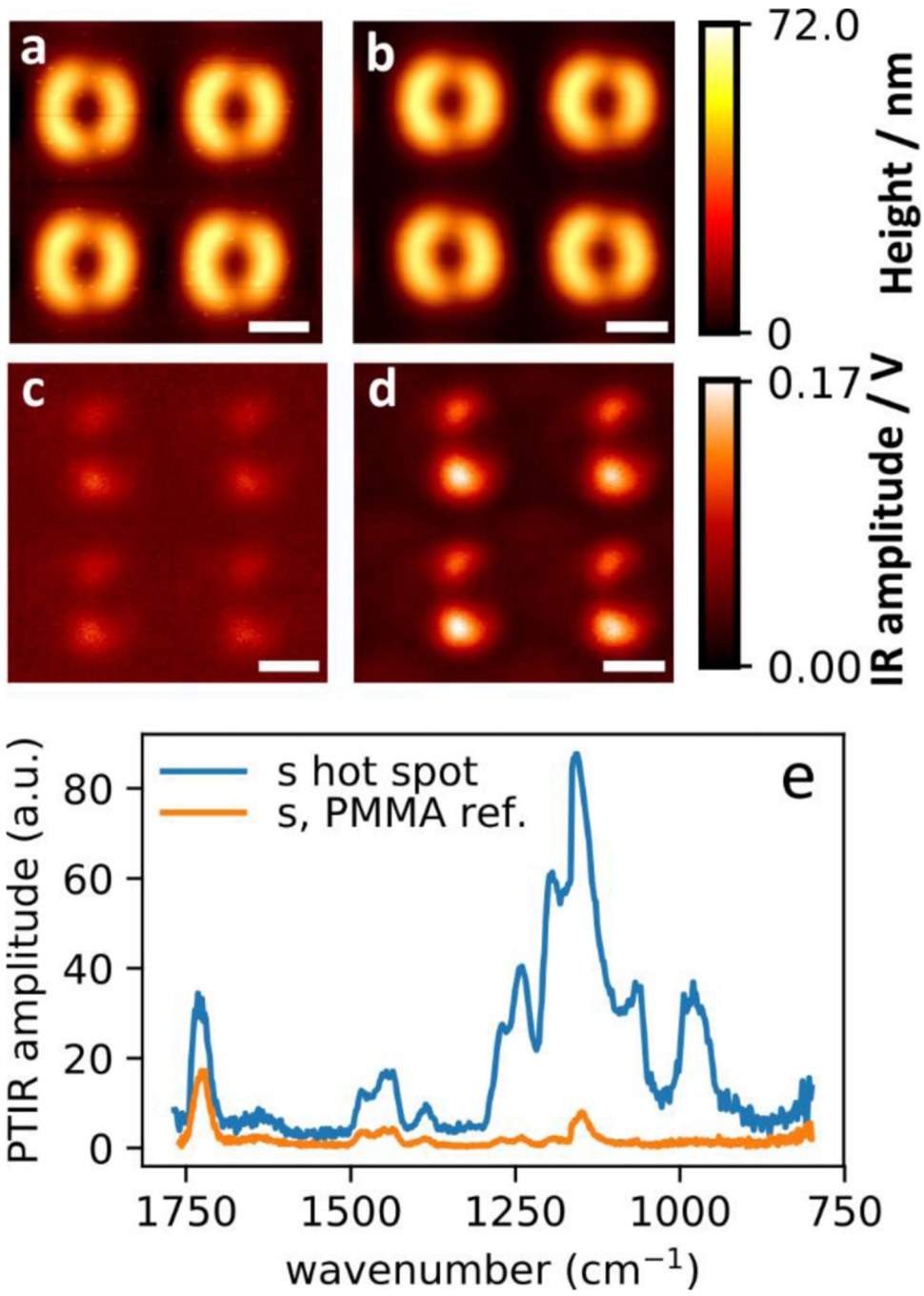

Figure 2. Comparison of PTIR measurement in air and water.

AFM topography images of gold plasmonic resonators coated with 200 nm PMMA layer in air (a) and water (b). Corresponding PTIR absorption images (1188 cm^{-1}) in air (c) and water (d). All images were obtained using s-polarized light. All scale bars are 1.0 μm (e) Comparison of representative PTIR spectra in water obtained from a hotspot location and on the PMMA film away from the resonator (reference).

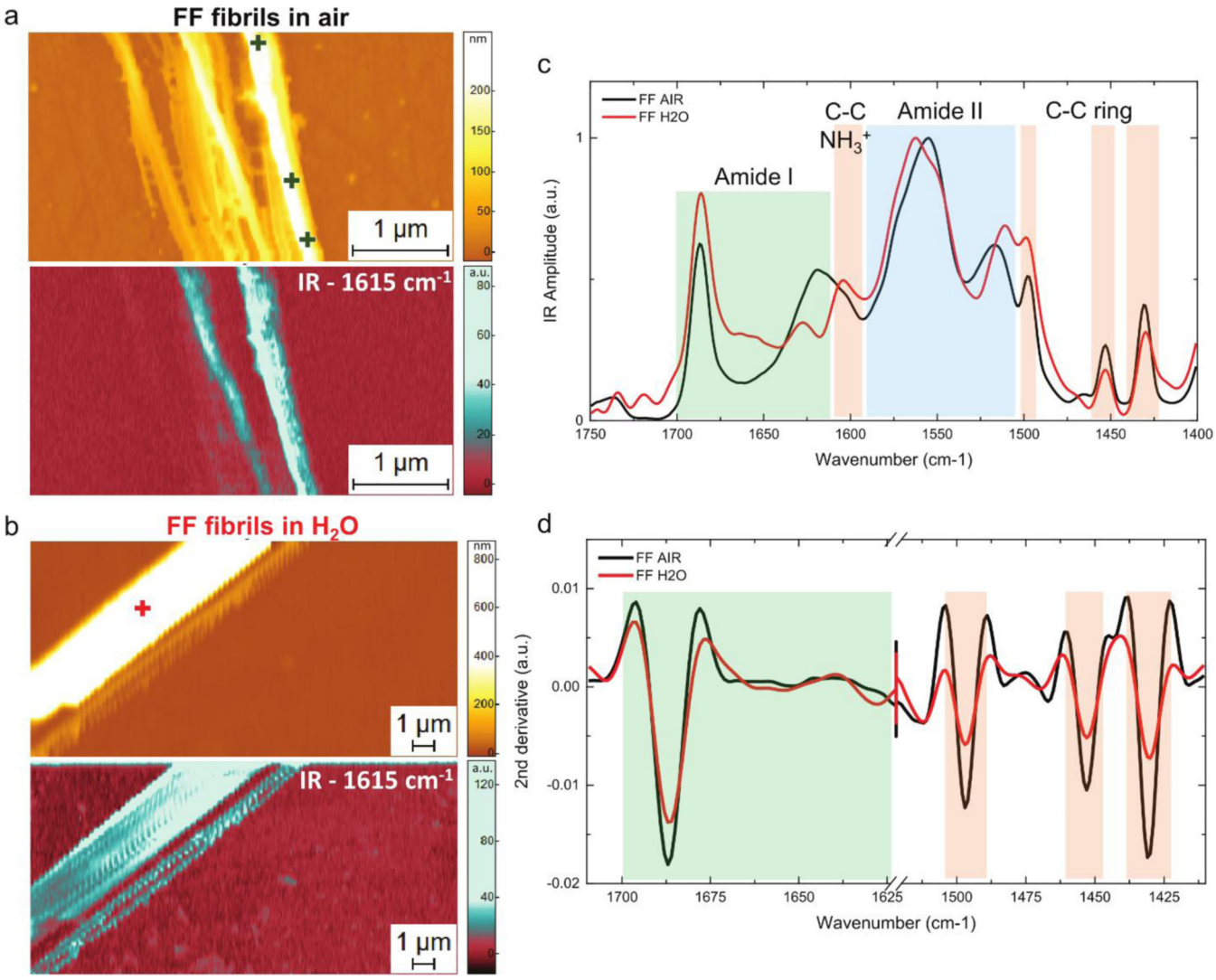

Figure 3. PTIR measurement of FF fibrils in air and H_2O.

Morphology and IR absorption map (1615 cm^{-1}) for FF fibrils in a) air and b) H_2O. c) Comparison of the average PTIR spectra covering the Amide I band (green), amide II (blue) and C-C ring (orange) spectral regions. The + symbols mark the locations where the individual spectra reported in the SI Figs 2–3 where acquired. d) Comparison of the second derivatives of the spectra in the Amide band I and C-C ring absorption.

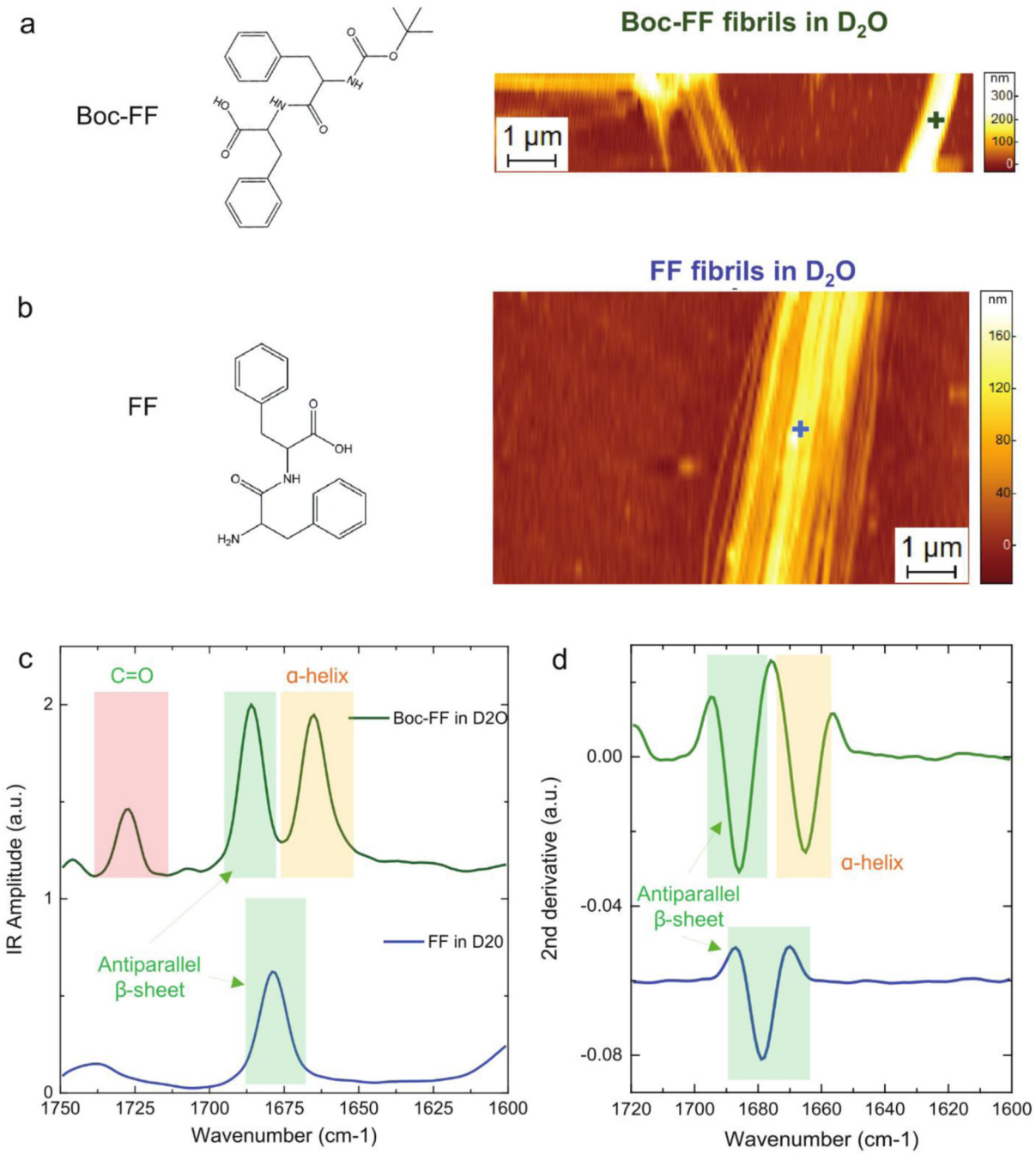

Figure 4. PTIR structural comparison of FF and Boc-FF fibrils in D_2O.

Chemical structure and AFM morphology map of a) Boc-FF and b) FF fibrils. c) Comparison of the fibrils average PTIR spectra in the Amide I (green and yellow) and C=O stretching vibration (red) spectral ranges. The + symbols mark the locations of the individually acquired spectra, reported in SI Fig. 2–3. d) Comparison of the second derivatives spectra in the Amide band I region.